Heliyon 9 (2023) e20900

Contents lists available at ScienceDirect

Heliyon

journal homepage: www.cell.com/heliyon

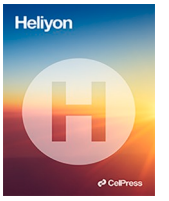

Improvement and application of electromagnetic vibration and noise suppression method for electric vehicle motor

Xuehui Lou, Shangyue Zhang, Xiaoqiang Chen, Yun Gao *, Wujun Ji

Henan Polytechnic, Zhengzhou, 450046, China

A R T I C L E I N F O

Keywords:
Electric vehicle
Induction motor
Electromagnetic vibration
Noise suppression
Motor torque

A B S T R A C T

Motor induced Electromagnetic Vibration and Noise (EVN) are mainly affected by Radial Electromagnetic Force Wave (REFW) and related harmonic amplitude. Therefore, in the past discussion on the suppression of motor induced EVN, it usually starts from this aspect. For this reason, this study proposes a method to suppress EVN. Firstly, the influence of the quantity of rotor slots on the function of Induction Motor (IM) is analyzed; Then, the optimization strategy of rotor slot fit is proposed according to the results; Finally, an optimization strategy for the skewness of IM is proposed. Based on the above contents, the experiment realized the suppression of EVN induced by electric vehicle motor. The experimental results show that the parameters of the motor are optimal when the quantity of rotor slots is 53. It is better to weaken the harmonic amplitude related to the low-order REFW. The peak values of the motor using the research strategy at the second and third vibration modes are - 35 db Hz and - 38 db Hz respectively, which are lower than those of the traditional motor. To sum up, the strategies proposed in the study can remarkably suppress the EVN of IM and improve the function of electric vehicles, which will promote the electric vehicle industry ‘s development.

1. Introduction

In the process of the continuous enhancement of China’s economy, people’s living standards has been improving, and the number of car sales has also been increasing. In this context, the automobile market has developed rapidly and become an important part of China’s market economy [1]. Under the basic strategy of sustainable development, fuel vehicles are gradually withdrawing from the market. Electric vehicles using clean energy have gradually become the substitute for fuel vehicles, and become the common means of transportation for people’s daily travel [2–4]. IM with high stability, simple maintenance and low cost are usually used in electric vehicle drive systems. However, the EVN of IM will cause motor driving noise and affect passengers’ riding experience. Therefore, the noise suppression effect is a part of the essential indicators to estimate the comfort of electric vehicles [5,6]. The current research results have confirmed that the main cause of motor induced EVN is REFW. Therefore, weakening the REFW can weaken the EVN of the motor [7–12]. The radial electromagnetic force wave is closely related to the slot fit and the distance between the rotor slots. Thus, this study proposes strategies from the two angles of slot fit and rotor slot distance to suppress the EVN induced by the motor and improve the passenger’s riding experience and comfort. This strategy has a positive effect on the development of the electric vehicle market. There are two main innovations in the research. The first point is to improve the slot matching strategy of IM, and design a 36/53 slot matching IM to weaken the force wave amplitude; The second point is to propose a strategy to determine the rotor chute distance,

* Corresponding author.
E-mail address: gyauto@126.com (Y. Gao).

https://doi.org/10.1016/j.heliyon.2023.e20900
Received 23 March 2023; Received in revised form 14 September 2023; Accepted 10 October 2023
Available online 14 October 2023

which fills the gap in current research. Compared with existing strategies, the proposed strategy has simple implementation, lower technical requirements and costs, and significant suppression effects on electromagnetic vibration and noise. This research consists of four parts. The first is the analysis and elaboration of current relevant research; In the second part, the suppression methods of EVN of IM are proposed; The third part is to verify the performance of the methods suggested in this study; The last part is the summary of the research content. The main contribution of the research is to verify the irrationality of the current design of induction motors and provide corresponding design improvement strategies, thereby weakening the electromagnetic vibration and noise of induction motors.

2. Related works

The components of IM include stator and rotor. Because its rotor speed is not synchronous with the rotating speed of the magnetic field, it is also called asynchronous motor. The IM has the features of high stability, simple maintenance, low cost. It is often applied as the driving system of electric vehicles, water pumps and other equipment, and is the basis of the development of the electric vehicle industry. For this reason, many researchers have conducted in-depth research on IM. Hsu C H et al. developed a fractional order PID control method, which effectively reduced IM vibration and noise [13]. Zhou Y et al. designed a new type of rotor winding to reduce IM torque ripple and electromagnetic noise, and improve operational safety and comfort during driving. The experimental results showed that the rotor winding has a good suppression effect on IM torque ripple and electromagnetic noise [14]. Choudhary A et al. proposed an infrared thermal imaging method based on two-dimensional discrete wavelet transform (2D-DWT) to realize intelligent detection of bearing faults of IM [15]. Kumar P et al. made a comprehensive description of the research results recently, thus analyzing the feasibility of the intelligent fault detection technology of IM based on machine learning algorithm, which will promote the development of IM [16]. Zaman S M K et al. suggested a graph-based semi-supervised learning method to realize intelligent fault diagnosis of IM. This method improves the efficiency and accuracy of fault diagnosis of IM and ensures the safe operation of IM [17]. Abro K A et al. used the drilling system to drive AB – fractal – fractional differential to carry out numerical analysis and mathematical analysis of IM, providing a theoretical path for the application, improvement and development of IM [18]. Hadi Salih I et al. suggested a probabilistic neural network on the bias of deep learning technology. At the same time, an intelligent model is built based on probabilistic neural network to detect and classify the faults during the operation of the IM, so as to improve the operation stability of the IM [19]. Wu Y et al. carried out simulation analysis on the structure of squirrel cage IM of CRH train and summarized its common early winding fault types. The experiment puts forward corresponding fault detection and diagnosis methods, which improves the safety of CRH trains [20].

In electric vehicles, because the operation of the motor involves changes, and the changes in the electromagnetic field are prone to generate electromagnetic wave clutter signals, electromagnetic noise is often generated. Electromagnetic noise will interfere with the information acquisition of passengers and drivers, and also affect the passenger's riding experience [21–23]. Therefore, many scholars have proposed methods to eliminate electromagnetic noise. Wang Y S et al. built an acoustic model of permanent magnet synchronous motor (PMSM) for coupling simulation, aiming at the issue of serious electromagnetic noise in PMSM and affecting the comfort of electric vehicles. Feng L et al. proposed a low switching frequency model to predict and control the serious electromagnetic noise in IM, which affects the comfort of electric vehicles. The results show that the model has good noise control effect [24]. Yoon Y H et al. proposed a control algorithm to address the issue of high noise intensity in unilateral linear IM used for propulsion of semi high-speed maglev trains. The results showed that under the control of this algorithm, the noise of IM was significantly reduced [25]. Zerdali E et al. proposed an adaptive extended Kalman filter to predict and evaluate speed sensorless control applications of IM and effectively reduce electromagnetic noise [26]. Deng W et al. analyzed the operation mechanism of PMSM and studied the sideband electromagnetic noise caused by rotor position error in PMSM. The corresponding processing strategy is proposed in the experiment to reduce the sideband electromagnetic noise [27]. Dong Q et al. suggested a multi-physics finite element method to summarize the generation principle of EVN in PMSM. This research realizes the prediction and analysis of EVN in PMSM, and lays the foundation for EVN suppression of electric vehicle drive motor [28]. Wang Q et al. proposed a cascaded permanent magnet switched reluctance generator with high efficiency in view of the low efficiency of PMSM in electric vehicles and proposed a suppression strategy for its electromagnetic noise [29].

It can be seen from the above contents that the application of IM in electric vehicles is very common and extensive. In addition, the EVN of the drive motor are urgent problems to be solved. This issue is significant to the safety of electric vehicles and the experience of passengers. However, in the current research results, the effectiveness of electromagnetic noise suppression for induction motors is not ideal enough. In addition, the implementation of electromagnetic vibration and noise suppression strategies is currently difficult, costly, and mostly theoretical, with poor practicality. Therefore, this study proposes an EVN suppression strategy for electric vehicle IM to improve the vibration and noise suppression efficiency of IM, reduce costs, and to some extent promote the improvement of the electric vehicle industry.

3. EVN suppression strategy of IM

3.1. Influence of rotor slot number of IM on motor performance

It is verified that the slot fit design of IM is very important in electric vehicles, which directly affects the distribution of magnetic flux density and REFW in the air gap, and also indirectly affects the EVN of IM. Slot matching refers to the combination strategy of the number of stator slots and the number of rotor slots in an induction motor, that is, the number of stator slots/the number of rotor slots.

The proper ratio of the stator slots' number and the rotor slots' number can reduce the EVN of the IM by weakening the electromagnetic force wave. Generally speaking, in IM of electric vehicles, the stator and rotor generally adopt 36/42 slot fit, as displayed in Table 1.

However, the slot fit in Table 1 will lead to low order REFW with fixed frequency in a certain range in the air gap of the motor, which will cause EVN of the motor. Thus the slot fit of IM needs to be optimized. In IM, the calculation of REFW is shown in formula (1).

$$p_r = \frac{b^2(\theta, t)}{2\mu_0} \tag{1}$$

In formula (1), p_r is the REFW; μ_0 is the air permeability; $b(\theta, t)$ denotes the air gap Magnetic Density (MD), T; θ represents the space mechanical angle; t denotes time. Many studies have shown that the stator slots' quantity only affects the order of REFW. The rotor slots' quantity will not only affect the order of the REFW, but also affect the frequency of the electromagnetic force wave. Therefore, the rotor slots' quantity has a greater impact on EVN in the motor. The research adopts the strategy that stator slots' quantity remains unchanged and only the rotor slots' quantity is changed to optimize the slot fit of IM. In the performance evaluation of IM of electric vehicle, the maximum electromagnetic torque $T_{\max}$ is one of the most important indicators, which has a great correlation with the starting ability and climbing ability of the vehicle. The maximum electromagnetic torque $T_{\max}$ can be calculated by formula (2).

$$T_{\max} = \frac{3pU^2}{4\pi f\left[R_1 + \sqrt{R_1^2 + \left(X_{1\sigma}^{'} + X_{2\sigma}^{'}\right)^2}\right]} \tag{2}$$

In formula (2), $R_1, X_{1\sigma}^{'}$ is the resistance and leakage reactance of the stator of the IM; $X_{2\sigma}^{'}$ is the converted value of rotor leakage reactance. According to formula (2), the rotor leakage reactance greatly influence the electromagnetic torque of IM. Slot leakage reactance, end leakage reactance and harmonic leakage reactance form the Rotor leakage reactance. Rotor slot leakage reactance $X_{s2}^{'}$ can be calculated according to formula (3).

$$X_{s2}^{'} = \frac{m \cdot p \cdot \lambda_{s2} \cdot l_2}{l_{ef} Z_2} C_X \tag{3}$$

In formula (3), m is the phase number of the IM; p is the quantity of motor poles; λ_{s2} is the unit leakage bayonet; l_2 represents the core length; l_{ef} denotes the core length; Z_2 denotes the number. According to formula (3), when the quantity of rotor slots increases, the leakage reactance of rotor slots decreases, and the electromagnetic torque increases. The rotor harmonic leakage reactance $X_{d2}^{'}$ can be calculated by formula (4).

$$X_{d2}^{'} = \mu_0 \frac{m \cdot \left(N_1 K_{dp1}\right)^2 p \cdot n_s}{9\delta_{ef}} \cdot \frac{D}{(Z_2)^2} \tag{4}$$

In formula (4), N_1 denotes the quantity of series turns of any phase of stator winding; K_{dp1} denotes the fundamental wave coefficient of stator winding; n_s denotes the synchronous speed of the IM; D represents the diameter; δ_{ef} is the effective air gap length of the motor. From formula (4), it can be seen that the number of rotor slots is inversely proportional to the harmonic leakage reactance, and directly proportional to the maximum electromagnetic torque of the motor, while the harmonic leakage reactance is directly proportional to the maximum electromagnetic torque. The air gap harmonic flux of the motor will cause additional losses, including surface loss and pulsation loss. Among them, the surface loss is related to P_B the quantity of stator slots and rotor slots of the motor, as shown in formula (5).

$$P_B \propto \frac{1}{Z^m}, m = 1.0 \sim 1.5 \tag{5}$$

In formula (5), Z is the quantity of stator slots or rotor slots. The surface loss of the motor has a negative correlation with the quantity of rotor slots. The pulsation loss P_m is related to the matching of motor slot, as shown in formula (6).

$$P_m = \frac{Z_2}{Z_1} \sin \frac{Z_1}{Z_2} \tag{6}$$

Table 1
Basic parameters of IM.

Parameter	Code	Numerical value	Parameter	Code	Numerical value
Rated voltage	U_{AC}	51 V	Number of stator slots	Z_1	36
Rated power	P_1	10 KW	Outer diameter of rotor	R_3	108.6 mm
Peak power	P_2	30 KW	Rotor inner diameter	R_4	38 mm
Speed range	n	0–6000 rpm	Number of rotor slots	Z_2	42
Polar logarithm	p	2	Core length	L	180 mm
Outer diameter of stator	R_1	188 mm	Peak torque	$T_{\max}$	116 N·m
Stator Bore	R_2	110 mm	Maximum speed torque	T_h	46 N·m

From formula (6), the difference between the stator slots' quantity and the rotor slots' quantity decreases with the pulsation loss decreasing. The increase of the rotor slots' quantity can increase $T_{\max}$, decrease P_B and increase P_m of the IM. Because the drive function of IM is more important, the increase of rotor slot number is conducive to the improvement of motor performance.

3.2. Optimization strategy for slot matching of IM

According to the above analysis, a slot-fit strategy is proposed to suppress the EVN of the motor on the premise of ensuring the driving performance of the motor. Considering the mechanical strength of the rotor, the number of rotor slots is initially set to 47–54 [30]. The synchronous additional torque will increase the motor loss, so the suppression of synchronous additional torque should be considering when setting the number of rotor slots. Make the number of rotor slots meet formula (7) to suppress the synchronous additional torque caused by low-order tooth harmonics.

$$\begin{cases} Z_1 \neq Z_2 \\ Z_1 - Z_2 \neq \pm p \\ Z_1 - Z_2 \neq \pm 2p \end{cases} \tag{7}$$

Make the number of rotor slots meet formula (8) to suppress the synchronous additional torque generated by the first-order tooth harmonic of the rotor and the phase band harmonic of the stator winding.

$$\begin{cases} Z_2 \neq 2pmk \\ Z_2 \neq 2pmk \pm 2p \end{cases}, k = 1, 2.3\ldots \tag{8}$$

According to the simultaneous formula (7) and formula (8), $Z_2 \neq 48, 52$, so its value is 47,49,50,51,53,54. The REFW generated by the motor with different rotor slot numbers is analyzed using the force wave table. See Table 2 for the analysis results.

When the order of the REFW is close to the vibration mode of the motor, or the frequency of the force wave is close to the frequency of the motor, the REFW will cause serious EVN of the motor [31–33]. The modal analysis of the IM is carried out by using finite element analysis, and its second and third mode shapes are shown in Fig. 1. It can be seen that in the same mode, the motor has multiple natural frequencies, which is because the overall structure of the induction motor is relatively complex. In addition, the natural frequency of the second mode vibration of the induction motor is significantly lower than that of the third mode vibration.

As shown in Fig. 1, (a), (b), (b), (c) and (d) are the 2-order mode patterns and their inherent frequency analysis results of the whole induction motor. Fig. 1: (e), (f), (g) and (h) are the results of the third order mode vibration pattern and its natural frequency analysis of the whole induction motor. The IM's natural frequency of the first order vibration mode is usually higher than 8000Hz, and it is a one-way reciprocating vibration, which is greatly different from the frequency of the first order force wave. Therefore, the first order force wave will not cause the first order resonance. The second mode and natural frequency are very close to those of the second force wave, so the resonance effect is very obvious. In addition, the frequency range of the first order force wave coincides with the partial natural frequency range of the second order vibration mode of the motor, so the first order force wave will also cause the second order resonance. The third-order force wave will cause the third-order resonance of the motor. However, the force wave's amplitude decreases with the order decreasing, so the smaller the impact on the EVN of the motor. To sum up, the third-order force wave has the smallest impact on the EVN of the motor, followed by the first-order force wave, and the second-order force wave has the largest impact. After comprehensive consideration of the above contents, the EVN of the IM are the minimum when the slot fit is 36/51 and 36/53. Analyze the REFW under the cooperation of these two grooves, as shown in Table 3.

When the slot fit is 36/51, the third-order force wave is mainly produced by the combined action of the fourth-order stator harmonic and the first-order rotor harmonic. When the slot fit is 36/53, the third-order force wave is mainly produced by the combined action of the fifth-order stator harmonic and the first-order rotor harmonic. Based on the above, when the slot fit is 36/53, the amplitude and number of force waves in the motor are lower than the slot fit of 36/51. In addition, under the slot matching strategy, the harmonic pole number of the stator winding is large, which greatly reduces the force amplitude compared with the 36/42 slot matching strategy. Based on the above contents, the slot matching strategy is determined as 36/53, and the optimization and improvement of the slot matching strategy is completed.

Table 2
REFW analysis results.

Number of rotor slots	Number of first-order force waves	Number of second-order force waves	Number of third-order force waves	Number of 4th order force waves
47	2	–	–	–
49	2	–	–	–
50	–	2	–	–
51	1	–	2	–
53	1	–	1	–
54	–	2	–	–

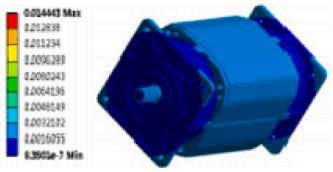

(a) 2nd mode vibration mode of induction motor 852 HZ

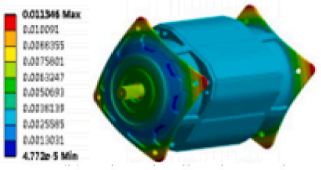

(b) 2nd mode vibration mode of induction motor 894 HZ

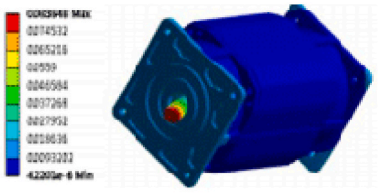

(c) 2nd mode vibration mode of induction motor 852 HZ

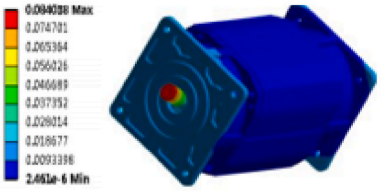

(d) 2nd mode vibration mode of induction motor 1162 HZ

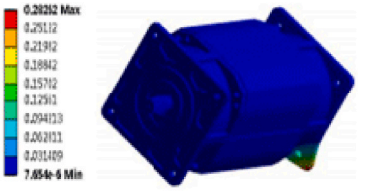

(e) 2nd mode vibration mode of induction motor 3196 HZ

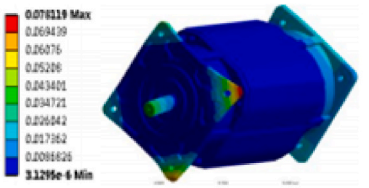

(f) 2nd mode vibration mode of induction motor 3467 HZ

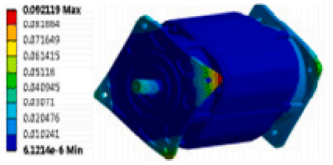

(g) 2nd mode vibration mode of induction motor 3783 HZ

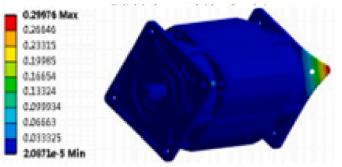

(h) 2nd mode vibration mode of induction motor 3897 HZ

Fig. 1. Modal analysis of IM.

Table 3
REFW with two grooves.

Stator winding harmonics			51 slot rotor harmonic polar pairs		53 slot rotor harmonic polar pairs	
Order	Harmonic number	Polar logarithm	−49	53	−51	55
4	23	−46	3	–	–	–
	25	50	1	3	−1	–
5	29	−58	–	–	–	−3
	31	62	–	–	–	–

3.3. Slotting optimization strategy of IM

In the previous content, this study optimized the slot matching strategy. The experiment adopts 36/53 slot matching strategy to greatly reduce the amplitude of force wave, and then suppress EVN. Next, the research optimizes the rotor chute distance to further weaken the force amplitude value, so as to make the suppression effect of EVN better. In the existing research literature, rotor chute is a common method to suppress EVN, and has a relatively good effect. Its principle is that the rotor slot can weaken the harmonic, thus weakening the resonance of the motor, and finally achieve the effect of suppressing EVN. However, the current research has no clear result on the optimal distance of the rotor chute, so the weakening effect of the force wave may not be the best. For this reason, a strategy is constructed to decide the optimal chute distance of the IM. Suppose that the sub-harmonic winding coefficient of the stator v' is $K_{dpv'}$ when the IM rotor does not adopt the slot strategy, and the sub-harmonic winding coefficient of the stator v' is $K_{dpcv'}$ when the IM rotor adopts the slot strategy and the slot degree is C, then there is formula (9).

$$K_{dpcv'} = K_{dpv'} \cdot K_{cv'} \tag{9}$$

In formula (9), $K_{cv'}$ means that when the IM rotor adopts the slot strategy and the slot degree is C, the slot coefficient of the sub-harmonic of the stator v' can be calculated by formula (10).

$$K_{cv'} = \frac{\sin\left(v' \cdot C \cdot \frac{\pi}{6q}\right)}{v' \cdot C \cdot \frac{\pi}{6q}} \tag{10}$$

If the slope is C, it can be calculated according to formula (11).

$$C = \frac{b_{sk}}{t_1} \tag{11}$$

In formula (11), b_{sk} is the distance of the chute; t_1 represents the tooth pitch of the stator v'. Through formula (9), formula (10) and formula (11), the reduction of C to different harmonics can be calculated. When the value of C is too large, a large transverse current will be generated, and then an axial force will occur. This situation will reduce the torque of the motor, increase the additional loss, and affect the IM's overall performance. Based on the above, the value of C should not be too high. The value range is 0–2. The correlation between the value of C and $K_{cv'}$ is shown in Fig. 2.

In Fig. 2, when the value of C is 1, that is, the stator tooth pitch is 1 times, as shown in point a, the first order tooth harmonic of the air gap is significantly weakened. However, at this point, the weakening effect of the REFW of the first and third order of the IM is poor. When the value of is 1.2, that is, the stator tooth pitch is 1.2 times, as shown in point b. At this time, the weakening effect of the 1st order tooth harmonic of the air gap is not as good as that of point a, but the weakening effect of the 1st and 3rd order REFW of the IM is obviously better than that of point a. This shows that the amplitude value of radial electromagnetic force of the IM is significantly limited under the C value shown in point b, thus suppressing the resonance of the IM, and then suppressing the EVN of the IM. On the bias of the above contents, the induction EVN suppression of electric vehicle motor is completed.

4. Effectiveness analysis of EVN suppression strategy of IM

To verify the improvement effect of slot matching strategy proposed in the study on IM, the finite element model of IM with rotor slots of 47,49,50,51,53,54 is constructed using the finite element analysis model. During the modeling process, the opening width of the rotor slot is kept consistent to more intuitively observe the effect of the rotor slots' quantity on the IM. First, verify the rationality of the research design. The MD cloud 's biggest value in the IM is 2.3T, and Fig. 3 demonstrates the MD distribution of the IM with different rotor slots. Fig. 3 (a), (b), (c), (c), (d), (e) and (f) are the magnetic maps of the rotor grooves at 47,49,50,51,53 and 54, respectively. As shown in Fig. 3, the magnetic density distribution of the induction motor is relatively uniform under different rotor slot numbers. Under different rotor slots, the MD distribution of IM is uniform. The MD distributed at the stator and rotor teeth is close to 1.8T, and the MD distributed at the stator and rotor yoke is lower. The finite element analysis is in good agreement with the design. In addition, the more the number of rotor slots, the higher the MD of the rotor yoke, but both are lower than the MD of the stator and rotor teeth. In this case, the saturation state of the rotor yoke is always after the tooth. As the number of rotor slots increases, the magnetic density of the motor rotor yoke shows an increasing trend, but its magnetic density value is lower than that of the stator and rotor teeth, so the rotor yoke will not saturate before the teeth. The above results prove the rationality of the research design.

The REFW distribution of IM with different rotor slots is shown in Fig. 4. Fig. 4 (a), (b), (c), (d), (e), and (f) show the circular distribution of radial electromagnetic force waves along the motor at the number of rotor grooves of 47,49,50,51,53, and 54, respectively. As shown in Fig. 4, when the number of rotor slots increases, the REFW distribution in the IM becomes more uniform, and the amplitude of the REFW decreases gradually. As the number of rotor slots increases, the distribution of radial electromagnetic force waves in the motor air gap tends to be uniform, and the amplitude of radial electromagnetic force waves also decreases with the increase of rotor slots. This is because the effect of rotor slot on air gap magnetic conductivity decreases with the increase of rotor slot number. The more rotor slots, the lower the distortion rate of the air gap magnetic density waveform, making it difficult to generate

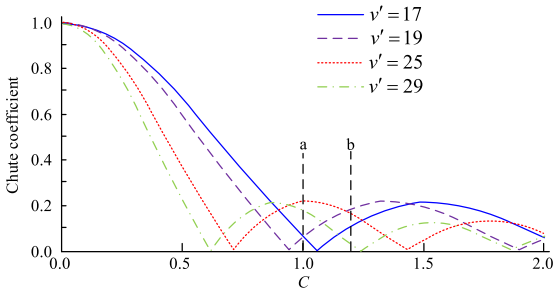

Fig. 2. Correlation between C and $K_{cv'}$.

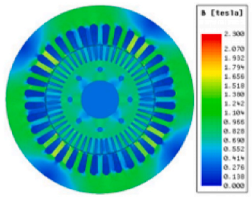

(a) 47 slot motor magnetic density cloud diagram

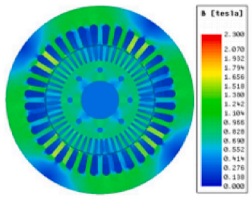

(b) 49 slot motor magnetic density cloud diagram

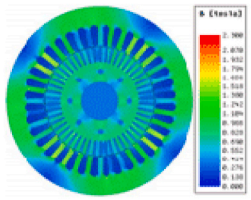

(c) 50 slot motor magnetic density cloud diagram

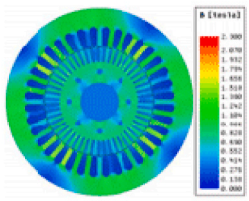

(d) 51 slot motor magnetic density cloud diagram

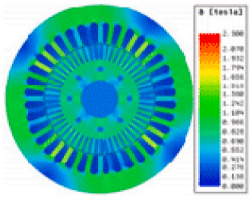

(e) 53 slot motor magnetic density cloud diagram

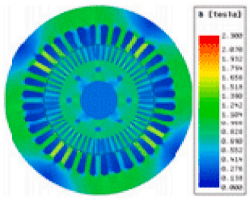

(d) 54 slot motor magnetic density cloud diagram

(caption on next page)

Fig. 3. MD distribution of IM with different rotor slots.

large "burrs" in its air gap magnetic density waveform. Therefore, increasing the number of slots in the motor rotor is beneficial for reducing the electromagnetic vibration and noise of the motor. This shows that the slot matching strategy proposed in the study can effectively suppress the electromagnetic force amplitude value in the IM, and then suppress the EVN of the IM.

Make the motor line current consistent. At the base speed point, Table 4 demonstrates the performance parameters of the IM with different rotor slots. When the rotor slots' quantity increases, the electromagnetic torque of the IM also increases, but the operating efficiency remains basically unchanged. When the rotor slots' quantity of IM exceeds 53, the electromagnetic torque has a slight downward trend. This means that when the rotor slots' quantity exceeds 53, increasing the number will not enhance the electromagnetic torque function of the motor. In addition, when the number of rotor slots is 53, the EVN of the motor can be minimized on the basis of ensuring the strength of the mechanical structure.

The motor line current is the same. The performance parameters of the IM with different rotor slots at the highest speed point are shown in Table 5. When the rotor slots' quantity increases, the electromagnetic torque of the IM also increases, but the operating efficiency remains basically unchanged. When the rotor slots' quantity of IM exceeds 53, the electromagnetic torque slightly increases. This means that when the rotor slots' quantity exceeds 53, it is invalid to enhance the electromagnetic torque function of the motor by changing the number. In addition, when the number of rotor slots is 53, the EVN of the motor can be minimized on the basis of ensuring the strength of the mechanical structure.

A rotor slot strategy is suggested to weaken the REFW, and the multi-section finite element simulation is used to analyze it, as shown in Fig. 5. Fig. 5 (a) is a schematic diagram of the oblique groove model. As shown in Fig. 5 (a), the research is to decompose the groove rotor into several sections along the motor axis, and treat each section as a straight groove motor, and each section is analyzed separately, and the analysis results are equivalent to the situation of the groove. Fig. 5 (b) for the multiple section finite element simulation diagram, as shown in Fig. 5 (b), the study can use the groove Angle and the ratio of rotor axial segments, representing the Angle of each segment, then use the software MotionSetup for the increasing Angle, the start of the groove can be simulated.

The simulation of 53-slot motors with C values of 1.0, 1.2 and rotor straight slot is carried out, and the FFT analysis of air-gap MD wave under different conditions is carried out. Fig. 6 (a) shows the results of the magnetic dense wave FFT analysis of the straight slot rotor. Fig. 6 (b) shows the results of FFT analysis of motor air gap magnetic dense wave when the rotor groove distance is 1 times the stator pitch is. Fig. 6 (c) shows the results of FFT analysis of the rotor groove distance is 1 times the stator tooth distance is demonstrates that when $C = 1$, the effect of weakening the 1st order tooth harmonic is very significant, but the effect of weakening the harmonic amplitude related to the lower order REFW is not obvious. When $C = 1.2$ is used, the effect of weakening the 1st order tooth harmonic is not as significant as when $C = 1$ is used, but the effect of weakening the harmonic amplitude related to the lower order REFW is better. These harmonics are the main factors that cause electromagnetic resonance and noise of the motor. Therefore, the EVN suppression effect of the motor at $C = 1.2$ is better.

To test the proposed strategy, the motor speed is set to 3000–6000 rpm. One of the motors is improved by the strategy proposed in the study, i.e. the slot ratio is 36/53, $C = 1.2$, the vibration frequency spectrum is shown in Fig. 7 (a); The other motor does not intervene. The slot ratio is 36/42, and the rotor slot is straight, the vibration frequency spectrum is shown in Fig. 7 (b). As can be seen from Fig. 7, the peak values of the motor using the research strategy at the second and third vibration modes are – 35 db Hz and – 38 db Hz, respectively, which are 5 db Hz and 18 db Hz lower than the original strategy. Based on the above, the proposed strategy can effectively reduce the amplitude of REFW and related harmonics in the motor to suppress the EVN of the IM.

5. Conclusion

EVN generated by IM due to REFW and related harmonics will affect the passenger's riding experience. In view of the above problems, the optimization strategy of slot fit and slot degree of IM is proposed. It is verified that at the base speed point, when the number of rotor slots increases, the REFW distribution in the IM becomes more uniform, and the amplitude of the REFW gradually decreases. When the rotor slots' quantity is 53, the EVN of the motor can be minimized on the basis of ensuring the strength of the mechanical structure. At this time, the motor's electromagnetic torque of is 120.128 N • m, the line current is 501.057 A, and the efficiency is 83.161 %. At the highest speed point, when the rotor slots' quantity is 53, the electromagnetic torque of the motor is 49.642 N • m, the line current is 500.871 A, and the efficiency is 84.978 %. All parameters are better than the number of other rotor slots. The above results verify the effectiveness of the 36/53 slot matching strategy proposed in the study. The effect of weakening the harmonic amplitude related to the low-order REFW is better, which verifies the usefulness of the suggested optimization strategy for the skewness of IM. The peak values of the motor using the research strategy at the second and third vibration modes are – 35 db Hz and – 38 db Hz, respectively, which are 5 db Hz and 18 db Hz lower than the original strategy. Based on the above, the proposed strategy can effectively decrease the amplitude of REFW and related harmonics in the motor to suppress the EVN of the IM. The study only conducted simulation analysis on the optimization strategy, and did not verify its effectiveness in suppressing electromagnetic vibration and noise during the actual driving process of electric vehicles. Therefore, it is necessary to conduct actual vehicle testing in subsequent research. In addition, the proposed strategy can only partially eliminate electromagnetic noise and cannot achieve complete elimination, so its application has certain limitations.

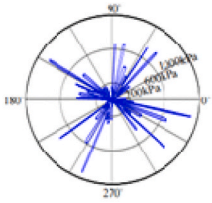

(a) Radial electromagnetic force wave of 47 slot motor

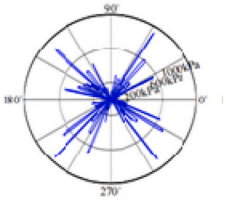

(b) Radial electromagnetic force wave of 49 slot motor

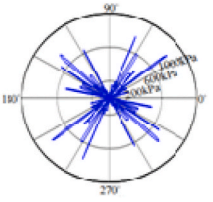

(c) Radial electromagnetic force wave of 50 slot motor

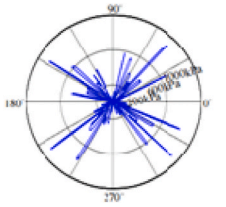

(d) Radial electromagnetic force wave of 51 slot motor

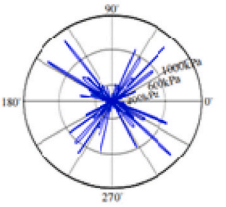

(e) Radial electromagnetic force wave of 53 slot motor

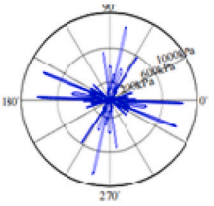

(f) Radial electromagnetic force wave of 54 slot motor

(caption on next page)

Fig. 4. REFW distribution of IM with different rotor slots.

Table 4
Performance parameters of IM with different rotor slots at base speed point.

Number of rotor slots	Performance parameters of IM		
	Electromagnetic torque (N·m)	Line current	Efficiency (%)
42	116.450	501.392	82.865
47	118.129	501.031	82.989
49	119.048	501.020	83.058
50	119.189	500.812	83.061
51	119.461	501.051	82.995
53	120.128	501.057	83.161
54	120.061	501.002	83.069

Table 5
Performance parameters of IM with different rotor slots at the highest speed point.

Number of rotor slots	Performance parameters of IM		
	Electromagnetic torque (N·m)	Line current	Efficiency (%)
42	46.172	500.918	84.289
47	48.279	500.958	84.779
49	48.688	500.820	84.888
50	48.989	500.982	84.890
51	49.158	500.828	84.869
53	49.642	500.871	84.978
54	49.718	500.896	84.898

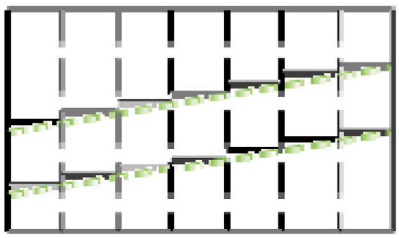

(a) Chute model simulation

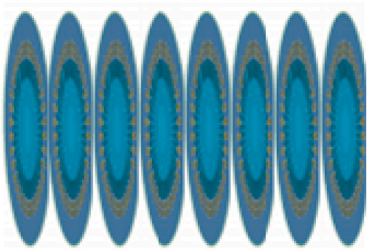

(b) Multi-section finite element simulation

Fig. 5. Multi-section finite element simulation.

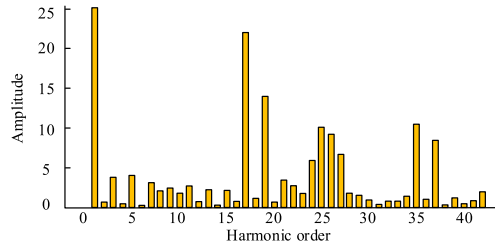

(a) Straight slot rotor air gap magnetic density FFT

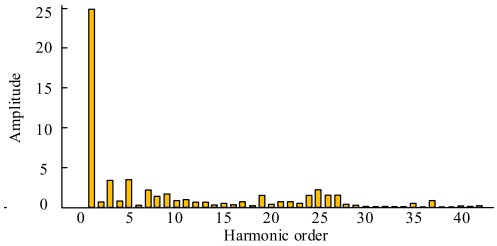

(b) $C=1$ rotor air gap magnetic density FFT

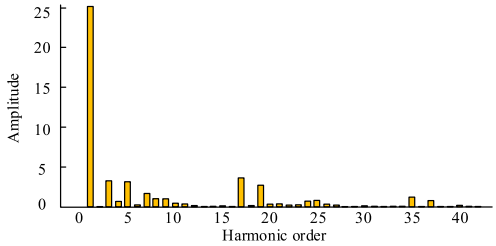

(c) $C=1.2$ rotor air gap magnetic density FFT

Fig. 6. FFT analysis of air-gap MD wave under different conditions.

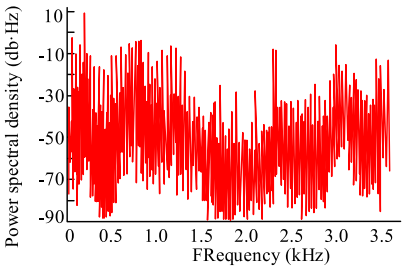

(a) Original configuration motor vibration spectrum

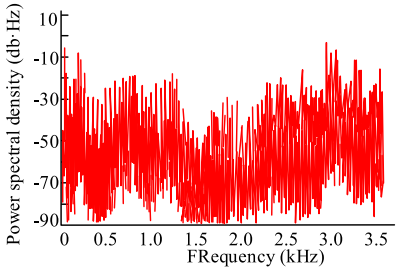

(b) Research strategy configuration motor vibration spectrum

Fig. 7. Study the effectiveness of proposed strategies.

Author contribution statement

Xuehui Lou: Conceived and designed the experiments; Wrote the paper. Shangyue Zhang: Xiaoqiang Chen: Performed the experiments; Analyzed and interpreted the data. Yun Gao: Conceived and designed the experiments. Wujun Ji:Contributed reagents, materials, analysis tools or data.

Data availability statement

Data included in article/supp. Material/referenced in article.

Declaration of competing interest

The authors declare that they have no known competing financial interests or personal relationships that could have appeared to influence the work reported in this paper.

References

[1] J.A. Sanguesa, V. Torres-Sanz, P. Garrido, F.J. Martinez, J.M. Marquez-Barja, A review on electric vehicles: technologies and challenges, Smart Cities 4 (1) (2021) 372–404.
[2] S. Acharya, Y. Dvorkin, H. Pandžić, R. Karri, Cybersecurity of smart electric vehicle charging: a power grid perspective, IEEE Access 8 (2020) 214434–214453.
[3] I. Miri, A. Fotouhi, N. Ewin, Electric vehicle energy consumption modelling and estimation—a case study, Int. J. Energy Res. 45 (1) (2021) 501–520.
[4] Y. Xiao, Y. Zhang, I. Kaku, R. Kang, X. Pan, Electric vehicle routing problem: a systematic review and a new comprehensive model with nonlinear energy recharging and consumption, Renew. Sustain. Energy Rev. 151 (2021), 111567.
[5] Z. Wang, T.W. Ching, S. Huang, H. Wang, T. Xu, Challenges faced by electric vehicle motors and their solutions, IEEE Access 9 (2020) 5228–5249.
[6] H.G. Min, Y.K. Fang, X. Wu, X.P. Lei, S.X. Chen, R. Teixeira, B. Zhu, X.M. Zhao, A fault diagnosis framework for autonomous vehicles with sensor self-diagnosis, Expert Syst. Appl. (2023), 120002.
[7] Y. Gao, M. Doppelbauer, J. Ou, R. Qu, Design of a double-side flux modulation permanent magnet machine for servo application, IEEE Journal of Emerging and Selected Topics in Power Electronics 10 (2) (2021) 1671–1682.
[8] S. Liu, Z. Song, Z. Dong, Y. Liu, C. Liu, Generic carrier-based pwm solution for series-end winding PMSM traction system with adaptative overmodulation scheme, IEEE Transactions on Transportation Electrification (2022) 1.
[9] S. Liu, C. Liu, Direct harmonic current control scheme for dual three-phase pmsm drive system, IEEE Trans. Power Electron. 36 (10) (2021) 11647–11657.
[10] J. Hu, Y. Wu, T. Li, B.K. Ghosh, Consensus control of general linear multiagent systems with antagonistic interactions and communication noises, IEEE Trans. Automat. Control 64 (5) (2019) 2122–2127.
[11] M. Ehsani, K.V. Singh, H.O. Bansal, R.T. Mehrjardi, State of the art and trends in electric and hybrid electric vehicles, Proc. IEEE 109 (6) (2021) 967–984.
[12] X. Zhang, Z. Lu, X. Yuan, Y. Wang, X. Shen, L2-gain adaptive robust control for hybrid energy storage system in electric vehicles, IEEE Trans. Power Electron. 36 (6) (2021) 7319–7332.
[13] C.H. Hsu, Fractional order PID control for reduction of vibration and noise on induction motor, IEEE Trans. Magn. (99) (2019) 1–7.
[14] Y. Zhou, X. Bao, W. Jiang, J. Liu, W. Xu, Novel rotor winding investigation for reduction of torque pulsation and electromagnetic noise in squirrel cage induction motor, Journal of Magnetics 24 (1) (2019) 135–141.
[15] A. Choudhary, D. Goyal, S.S. Letha, Infrared thermography-based fault diagnosis of induction motor bearings using machine learning, IEEE Sensor. J. 21 (2) (2020) 1727–1734.
[16] P. Kumar, A.S. Hati, Review on machine learning algorithm based fault detection in induction motors, Arch. Comput. Methods Eng. 28 (2021) 1929–1940.
[17] S.M.K. Zaman, X. Liang, An effective induction motor fault diagnosis approach using graph-based semi-supervised learning, IEEE Access 9 (2021) 7471–7482.
[18] K.A. Abro, A. Atangana, Numerical and mathematical analysis of induction motor by means of AB–fractal–fractional differentiation actuated by drilling system, Numer. Methods Part. Differ. Equ. 38 (3) (2022) 293–307.
[19] I. Hadi Salih, G. Babu Loganathan, Induction motor fault monitoring and fault classification using deep learning probablistic neural network, Solid State Technol. 63 (6) (2020) 2196–2213.
[20] Y. Wu, B. Jiang, Y. Wang, Incipient winding fault detection and diagnosis for squirrel-cage induction motors equipped on CRH trains, ISA Trans. 99 (2020) 488–495.
[21] S. Liu, C. Liu, H. Zhao, Y. Liu, Z. Dong, Improved flux weakening control strategy for five-phase PMSM considering harmonic voltage vectors, IEEE Trans. Power Electron. 37 (9) (2022) 10967–10980.
[22] X. Xu, Y. Sun, X. Tian, L. Zhou, Y. Li, A novel orientation determination approach of mobile robot using inertial and magnetic sensors, IEEE Trans. Ind. Electron. 70 (4) (2023) 4267–4277.
[23] W. Hu, T. Wang, F. Chu, A novel Ramanujan digital twin for motor periodic fault monitoring and detection, IEEE Trans. Ind. Inf. (2023), https://doi.org/10.1109/TII.2023.3248110.
[24] L. Feng, H. Yang, W. Song, Acoustic noise of induction motor with low-frequency model predictive control, IEEE Access 8 (2020) 178238–178247.
[25] Y.H. Yoon, Vibration and noise analysis of switched reluctance motor drive converter, Trans. Korean Inst. Electr. Eng. 68 (3) (2019) 507–512.
[26] E. Zerdali, Adaptive extended kalman filter for speed-sensorless control of induction motors, IEEE Trans. Energy Convers. 34 (2) (2019) 789–800.
[27] W. Deng, S. Zuo, Analysis of the sideband electromagnetic noise in permanent magnet synchronous motors generated by rotor position error, IEEE Trans. Ind. Electron. 69 (5) (2021) 4460–4471.
[28] Q. Dong, X. Liu, H. Qi, Y. Zhou, Vibro-acoustic prediction and evaluation of permanent magnet synchronous motors, Proc. Inst. Mech. Eng. - Part D J. Automob. Eng. 234 (12) (2020) 2783–2793.
[29] Q. Wang, X. Li, X. Jing, W. Jiang, H. Jin, M. Li, Y. Chen, Control of a cascaded permanent magnet switched reluctance generator for automobile generation application, IEEE Access 9 (2021) 132830–132838.
[30] G. Li, Z. Fu, Y. Wang, Electromagnetic vibration and noise suppression of induction motor based on RPWM selective spectrum shaping, IEEE Access 9 (2021) 54509–54517.
[31] Y. Lu, C. Tan, W. Ge, Y. Zhao, G. Wang, Adaptive disturbance observer-based improved super-twisting sliding mode control for electromagnetic direct-drive pump, Smart Mater. Struct. 32 (1) (2023), 17001.
[32] D. Hu, Y. Wang, J. Li, Q. Yang, J. Wang, Investigation of optimal operating temperature for the PEMFC and its tracking control for energy saving in vehicle applications, Energy Convers. Manag. 249 (2021), 114842.
[33] D. Hu, S. Cheng, J. Zhou, et al., Energy management optimization method of plug-in hybrid electric bus based on incremental learning, IEEE Journal of Emerging and Selected Topics in Power Electronics 11 (1) (2021) 7–18.